Tunable RF MEMS Inductors for Two-Frequency Bands

HABBACHI NIZAR, BESBES KAMEL
Center for Research on Microelectronics & Nanotechnology,
CRMN 4050 Sousse,
TUNISIA

also with
Microelectronics and Instrumentation Laboratory,
Faculty of Sciences of Monastir,
University of Monastir,
5000 Monastir,
TUNISIA

Abstract: - This paper presents the design and simulation of two-variable MEMS inductors for high-frequency applications. In two cases, the inductors' cores are enclosed between two tunable metal plates. The medium permeability changes in response to iron plate movement, ensuring a high-tuning range above 250%. The first inductor is designed for the 10 GHz range, and the inductance value is comprised of Lmin = 3.37 nH and increases to Lmax = 11.8 nH. Similar inductance values are obtained for the second inductor, but it is designed to work at 20 GHz. Furthermore, the maximum value of the quality factor of the second inductor is slightly higher than the first one and reaches Qmax = 17.5.

Key-Words: - Inductor, Controlled, Variable, Microwave, MEMS, Integrated, Spiral, Optimization.

Received: April 8, 2023. Revised: November 11, 2023. Accepted: December 12, 2023. Published: April 2, 2024.

1 Introduction

Integrated inductors are essential components in modern RF circuits and have been studied in several recent works, [1], [2], [3], [4], [5]. In the early development of variable inductors, switchable inductors were the first design choice as a means of varying inductance values. This was first done using MEMS micro-relays, which were used to change the effective number of coil turns. However, inductors' values are not continuously tuned. In addition, most of them suffered from a low Q factor due to the high contact resistance of micro-relays, which limited their use in RF applications. The first known improvements have used MOSFET switches, which ensure continuous inductance variation. With this technique, [6], a total range of 8–23 nH at 2.4 GHz was reached. However, the Q factor peak was relatively small due to switch losses. Afterward, in a later work, [7], by optimally calculating the inductor layout parameters, such as the coil dimensions, the spacing, and the turn number. They improved the Q factor by optimizing the design of switchable inductors.

Subsequently, in this paper, we present two continuous tunable inductors intended to be integrated into 10 GHz and 20 GHz synthesizers. We used an etched substrate in order to eliminate the current leakage effect and to insert a metal plate underneath the inductor core. The displacement of two metal plates increases the inductance tuning range and enlarges the resonant frequency response. In the first part, we extend the design and the variation principle using a 3D FEM tool. Then, we present the obtained results in two cases, essentially the quality factor and inductance value in response to frequency and metal plate distances. Finally, we discuss and compare our work with close literature works presenting the effects of actuation techniques on inductor performances.

2 Variation Principle

Variable MEMS inductors provide the flexibility and adaptability needed to meet the changing performance requirements of RF circuits. Each design method has advantages and disadvantages, and the optimal choice depends on system specifications and trade-offs between performance, design complexity, and power consumption. Continued research in this area is necessary to improve the performance and reduce the manufacturing costs of these critical components.

Our methodology is to eliminate parasites by etching the substrate and increasing the variation by using two actuated plates. Indeed, we ensure higher performances than geometry or permittivity methods.

The distance between the inductor core and the metal plate influences the medium permeability and the performance of the MEMS inductor. The induced current in a metal plate changes in response to displacement and excitation frequency. In our case, two metal plates are tuned to increase the induced current effect on the inductance value and to increase the tuning range. The inductor is supposed to be used in a frequency synthesizer working at 10 GHz and 20 GHz. Consequently, we have designed two spirals' inductors with a different number of turns. The second spiral inductor has 2.5 turns, and the spiral dimensions are optimized to allow maximum tuning range for 20 GHz applications, [8], [9], [10], [11], [12], [13].

3 Integrated Inductor Design

The proposed inductor in Figure 1 is designed using modulated 4.5 turns spaced by 2 µm. The width of each spiral increases by 5 µm and reaches 25 µm at the last spiral. The inductor coil layer is constituted of 4µm thick copper deposited on a silicon substrate. Figure 1 illustrates two technological aspects, the first one is presented from the three-dimensional perspective of a classic integrated inductor, and the second one shows an etched substrate known as a MEMS inductor.

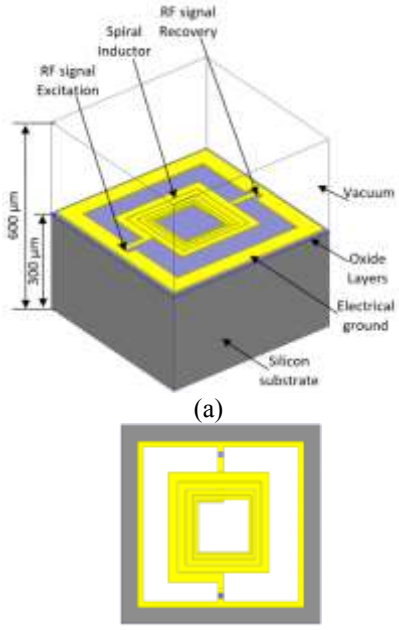

(a)

(b)

Fig. 1: (a) 3D perspective of spiral inductor (b) RF MEMS spiral inductor

To evaluate the inductors' performances, we used a FEM tool at frequencies between 0.1 GHz and 20 GHz. The determination of the inductance value and its quality factor can be calculated by the following equations:

$$y_1 = S_{11} - \left(\frac{S_{11}*S_{21}}{1+S_{22}}\right) \quad (1)$$

$$y_2 = S_{22} - \left(\frac{S_{12}*S_{21}}{1+S_{11}}\right) \quad (2)$$

$$Z_a = \left(\frac{1+y_1}{1-y_1}\right) \quad (3)$$

$$Z_b = \left(\frac{1+y_2}{1-y_2}\right) \quad (4)$$

$$ind = \left(\frac{Im(Z_a)+Im(Z_b)}{2\Pi f}\right) \quad (5)$$

$$Q = \left(\frac{Im(Z_a)+Im(Z_b)}{Re(Z_a)*Re(Z_b)}\right) \quad (6)$$

The obtained results of both structures are illustrated in Figure 2.

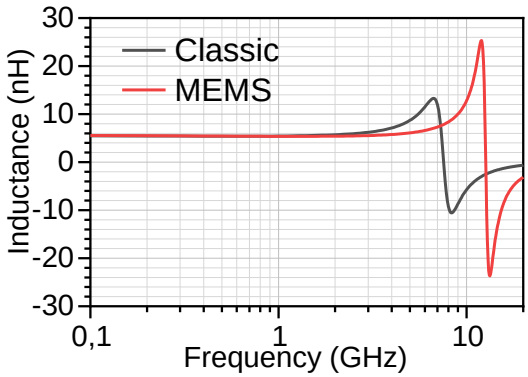

(a)

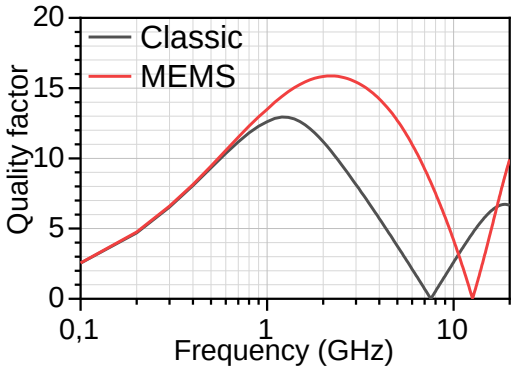

(b)

Fig. 2: Inductors performances in response to frequency variation (a) inductance value (b) quality factor

In two cases, the inductance increases in response to frequency and reaches a limit of self-resonant frequency, respectively, at 7.5 GHz for the classic inductor and 12.6 GHz for the MEMS inductor. Furthermore, as we can see in Figure 2(b), we obtain an important amelioration in quality factor value using an etched substrate: Qmax=15.9 at 2.2 GHz. This quality factor value is due to the limitation of parasitic effects of the silicon substrate

in a classic inductor, and the maximal quality factor was Qmax=12.9 and obtained at 1.2 GHz.

4 10 GHz Inductor Design

To ameliorate the performance of the MEMS inductor, we have enclosed the spiral coil with two metal plates as shown in Figure 3. The displacement interval of two plates is between 50 µm and 150 µm. The technological characteristics of the used iron are: conductivity is equal to σ = 10.3E6 S/m, and magnetic permeability is equal to µr=4000. Their geometric dimensions are as follows: length and width are equal to 215 µm and thickness is equal to 10 µm. The presented spiral inductor in Figure 3 is designed to be used for 10 GHz applications, [14], [15], [16], [17], [18], [19], [20].

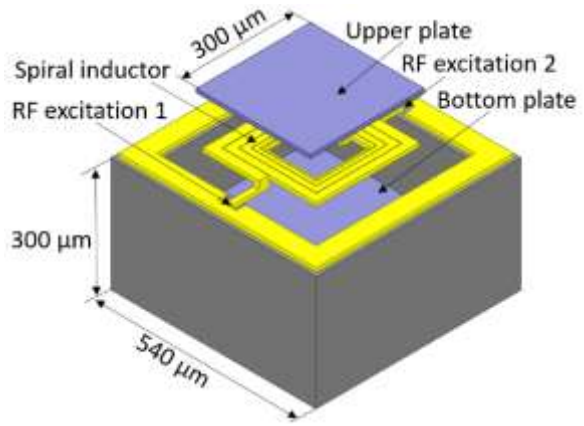

Fig. 3: 3D perspective of 4.5 turns MEMS inductor

We have plotted in Figure 4 the variation curves of inductance and quality factor as a function of frequency for six positions of the iron plates enclosing the inductor core:

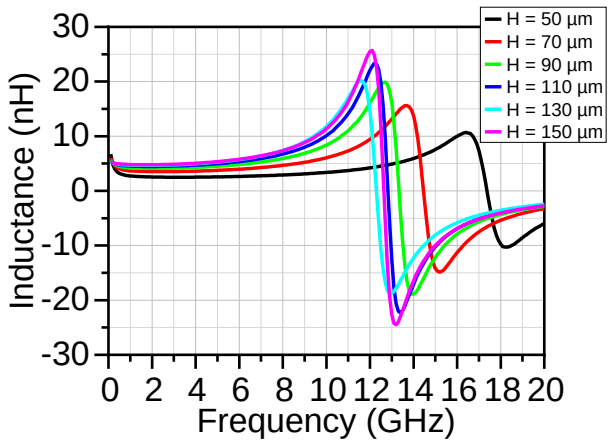

(a)

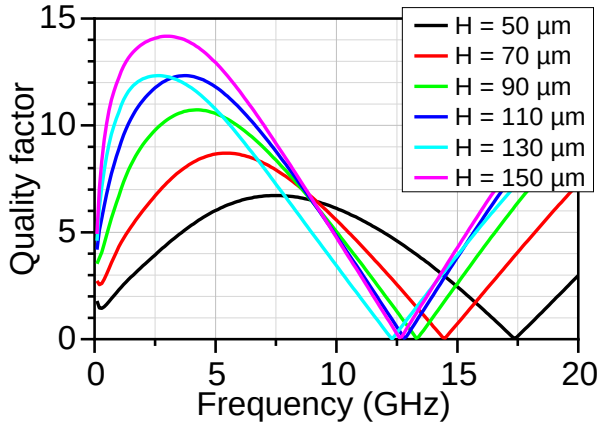

(b)

Fig. 4: Inductor performances in response to frequency :(a) inductance value, (b) quality factor

When the metal plates are closer to the inductor core, in our case the first distance is 50 µm, the resonant frequency increases and reaches 17.5 GHz. Nevertheless, the quality factor decreases when the metal plate distance is closer, and the maximum quality factor reaches 14.2 at the last distance is 150 µm. For this first 4.5T inductor, the tuning range at 10 GHz is lower than that obtained at 20 GHz, and for this reason, we have designed the second spiral inductor shown in the next paragraph.

5 20 GHz Inductor Design

In this design, we have used a 2.5T spiral MEMS inductor enclosed by two iron plates. In the same way, the two-plate displacement interval is between 50 µm and 150 µm. Figure 5 shows the 3D perspective view of the 2.5T spiral MEMS inductor enclosed by two metal plates:

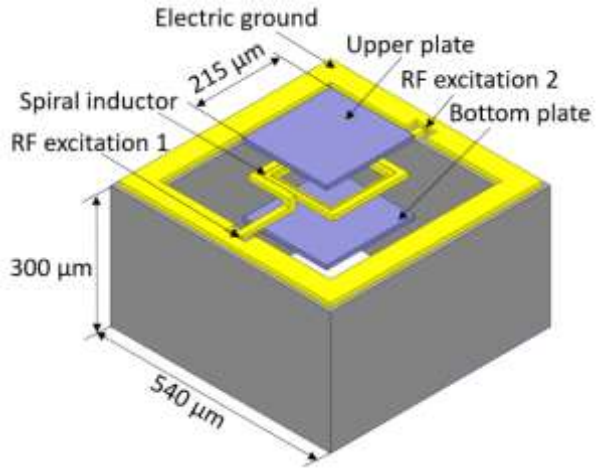

Fig. 5: The 3D perspective of 2.5 turns MEMS inductor

We have plotted in Figure 6 the variation curves of inductance and quality factor as a function of frequency for six positions of the iron plates enclosing the inductor core:

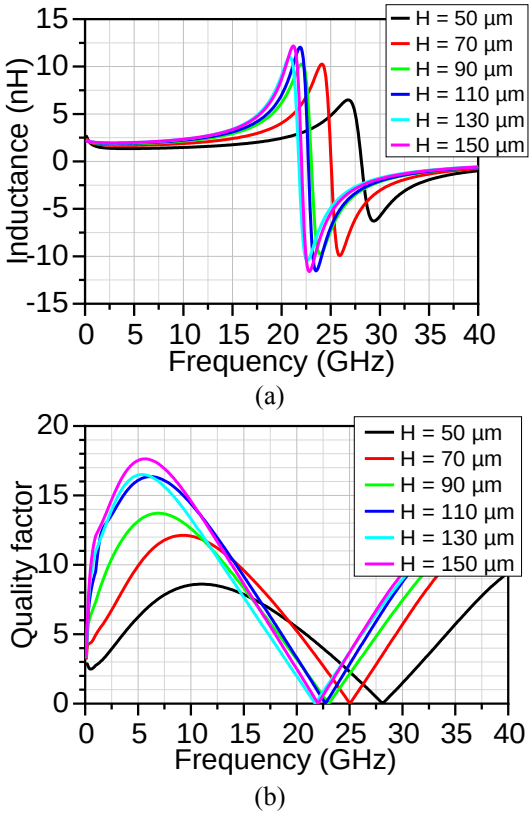

Fig. 6: Inductor performances in response to frequency :(a) inductance value, (b) quality factor

It is clearly seen that the second spiral inductor has the same performance behavior as the first one, in spite of the fact that the resonant frequency is much higher. Indeed, the metal plate distance is inversely proportional to the frequency response, allowing for an increase in the quality factor Qmax = 17.8. Nevertheless, the tuning range at 10 GHz is higher than the second spiral inductor and reaches Tr = 250%. So, this 2.5T spiral inductor is designed to work at 20 GHz, where the tuning range reaches Tr = 272%, and it is Tr = 59% at 10 GHz.

6 MEMS Inductors Performance Comparisons

The Figure 7 presents the inductance value variation at 10 GHz for the first inductor and at 20 GHz for the second inductor. Furthermore, the resonant frequency in response to the metal plate displacement for two inductor cases is:

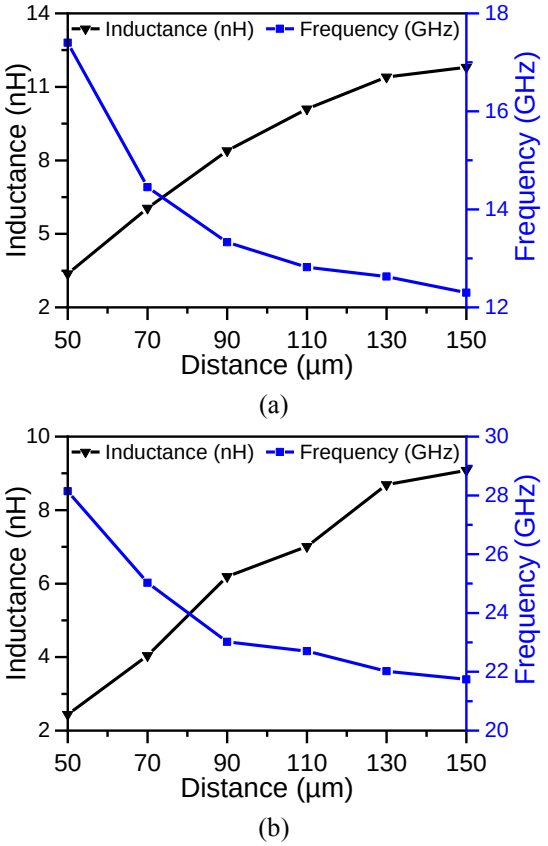

Fig. 7: Inductance value and resonant frequency variation in response to iron plate displacements (a) first design for 10 GHz (b) second design for 20 GHz

We note that in two cases, the inductance value variation is almost linear according to metal plate displacements. The second spiral inductor has better linearity variation than the first one, as illustrated in Figure 5(b). At the first position, the inductance value is minimal, and it gradually increases with the iron plate movements. Figure 5(b) shows that at 20 GHz, the inductance value is minimum (Lmin = 2.44 nH) and increases to Lmax = 9.08 nH, thus ensuring a high variation of Tr = 272%. Compared to the first 10 GHz inductor, the inductance value is at its minimum at Lmin = 3.37 nH and increases to Lmax = 11.8 nH with a very similar tuning range of Tr = 250%. However, the resonant frequency decreases, and it is comprised between 28,14 GHz and 21,74 GHz for the second design, and in the first case, the frequency range is comprised between 17.4 GHz and 12.3 GHz. In spite of this, in two cases, the frequency range is larger than 5 GHz, but it is still limited to a unique multi-band synthesizer.

In other forms of distance variation, a designed inductor is based on the modification of mutual inductance, [21]. A double-sided spiral inductor composed of aluminum and amorphous silicon (a-Si) was forced out of a silicon substrate. The

actuation phenomenon is due to the differences in CTE (Coefficients of Thermal Expansion) between aluminum and the a-Si layers. The increase in mutual inductance between inductors turns when the distances between them decrease as the structure flattens. During these transitions, the inductance value varied from 5.6 nH to 8.2 nH, indicating an adjustment range of 32%, and the maximum Q factor achieved was 15. By replacing spiral layers with porous anodic alumina (Al-PPA), the Q factor increased by 20, [22]. However, the adjustment range was reduced to 18%, and in addition, the deformation was rather arbitrary. Indeed, in our design, we fixed the inductor core and varied the medium permeability in order to control with accuracy and increase the inductance variation better than other previous works presented in the literature, [21], [22].

7 Conclusion

This paper demystifies the idea of designing the appropriate dispositive for a limited frequency range. Indeed, two continuous tunable inductors are designed to have the same inductance value range and are separated by 10 GHz in their frequency response. Each inductor serves a specific synthesizer RF application. In the second case, the obtained results show that the tuning range at 20 GHz is four times higher than that obtained at 10 GHz, with Tr = 272% and Tr = 59%, respectively, for the 20 GHz and 10 GHz designs. Thus, we have designed a 4.5T spiral MEMS inductor to respond to a large frequency difference at 10 GHz. The obtained results show comparable performances in the 10 GHz frequency range (Tr = 25%). This work would be helpful for RF circuit designers working on a multiband frequency synthesizer. In future work, we will incorporate those new structures into VCO architectures. Indeed, in previous work, we have developed VCO circuits using fixed inductors, and their tuning range is limited. Moreover, we are working on a new type of variable MEMS inductor using microfluidic actuation to increase the total tuning range of the presented inductors in this paper.

References:

[1] Rajni Prashar and G. Kapur, "On-Chip Tunable Active Inductor Circuit for Radio Frequency Ics," WSEAS Transactions on Electronics, vol. 14, pp. 91–103, Dec. 2023, https://doi.org/10.37394/232017.2023.14.11.

[2] J. Chatzakis, S. Hassan, E. Clark, M. Tatarakis "A 1GHz Low-cost, Ultra Low-noise Preamplifier," *WSEAS Transactions on Electronics*, vol. 11, Sep. 2020, https://doi.org/10.37394/232017.2020.11.15.

[3] Sabrije Osmanaj and Rexhep Selimaj, "Simulation and Design of an Integrated Planar Inductor Using Fabrication Technology," *WSEAS Transactions on Electronics*, vol. 8, Jan. 2017.

[4] N. Habbachi and K. Besbes, "Performance Evaluation of Microfluidically Tunable Microwave Filters," *Electronics*, vol. 11, no. 18, p. 2889, Sep. 2022, https://doi.org/10.3390/electronics11182889.

[5] N. Habbachi and K. Besbes, "RF MEMS filter based on dual liquid variations," *Journal of Micromechanics and Microengineering*, vol. 32, no. 6, p. 065002, Apr. 2022, https://doi.org/10.1088/1361-6439/ac6203.

[6] P. Park, C. S. Kim, M. Y. Park, S. D. Kim, and H. K. Yu, "Variable Inductance Multilayer Inductor With MOSFET Switch Control," *IEEE Electron Device Letters*, vol. 25, no. 3, pp. 144–146, Mar. 2004, https://doi.org/10.1109/led.2003.822670.

[7] A. Nieuwoudt and Y. Massoud, "Design optimization of switchable multi-port spiral inductors," *Analog Integrated Circuits and Signal Processing*, vol. 51, no. 3, pp. 195–200, Jun. 2007, https://doi.org/10.1007/s10470-007-9068-2.

[8] Meysam Bahmanian and J. Christoph Scheytt, "A 2–20-GHz Ultralow Phase Noise Signal Source Using a Microwave Oscillator Locked to a Mode-Locked Laser," *IEEE Transactions on Microwave Theory and Techniques*, vol. 69, no. 3, pp. 1635–1645, Mar. 2021, https://doi.org/10.1109/tmtt.2020.3047647.

[9] Y. Shu, Huizhen Jenny Qian, and X. Luo, "A Cascaded Mode-Switching Sub-Sampling PLL With Quadrature Dual-Mode Voltage Waveform-Shaping Oscillator," *IEEE Transactions on Circuits and Systems I-regular Papers*, vol. 68, no. 6, pp. 2341–2353, Jun. 2021, https://doi.org/10.1109/tcsi.2021.3063409.

[10] A. Bluestone, D. T. Spencer, S. Srinivasan, D. Guerra, J. E. Bowers, and L. Theogarajan, "An Ultra-Low Phase-Noise 20-GHz PLL Utilizing an Optoelectronic Voltage-Controlled Oscillator," *IEEE Transactions on Microwave Theory and Techniques*, vol. 63, no. 3, pp. 1046–1052, Mar. 2015, https://doi.org/10.1109/tmtt.2015.2397890.

[11] Teerachot Siriburanon, T. Sato, A. Musa, W. Deng, K. Okada, and A. Matsuzawa, "A 20GHz Push-Push Voltage-Controlled Oscillator Using Second-Harmonic Peaking Technique for a 60GHz Frequency Synthesizer," *IEICE Transactions on Electronics*, vol. E96.C, no. 6, pp. 804–812, Jan. 2013, https://doi.org/10.1587/transele.e96.c.804.

[12] Brian Sveistrup Jensen, M. M. Khafaji, T. K. Johansen, Viktor Krozer, and Johann-Christoph Scheytt, "Twelve-bit 20-GHz reduced size pipeline accumulator in 0.25µm SiGe:C technology for direct digital synthesiser applications," *IET circuits, devices & systems*, vol. 6, no. 1, pp. 19–19, Jan. 2012, https://doi.org/10.1049/iet-cds.2010.0399.

[13] Y. Wang, M. Katsuragi, K. Okada, and A. Matsuzawa, "A 20-GHz Differential Push-Push VCO for 60-GHz Frequency Synthesizer toward 256 QAM Wireless Transmission in 65-nm CMOS," *IEICE Transactions on Electronics*, vol. E100.C, no. 6, pp. 568–575, 2017, https://doi.org/10.1587/transele.e100.c.568.

[14] R. Navickas, "Design of Low Noise 10 GHz divide by 16…511 Frequency Divider," *Elektronika Ir Elektrotechnika*, vol. 19, no. 6, Jun. 2013, https://doi.org/10.5755/j01.eee.19.6.4570.

[15] S. Rong, J. Yin, and H. C. Luong, "A 0.05- to 10-GHz, 19- to 22-GHz, and 38- to 44-GHz Frequency Synthesizer for Software-Defined Radios in 0.13µm CMOS Process," IEEE Transactions on Circuits and Systems II: Express Briefs, Vol. 63, Issue: 1, January 2016, https://doi.org/10.1109/tcsii.2015.2482467.

[16] K. Raczkowski, N. Markulic, B. Hershberg, and J. Craninckx, "A 9.2–12.7 GHz Wideband Fractional-N Subsampling PLL in 28 nm CMOS With 280 fs RMS Jitter," *IEEE Journal of Solid-State Circuits*, vol. 50, no. 5, pp. 1203–1213, May 2015, https://doi.org/10.1109/jssc.2015.2403373.

[17] T.-Y. Lu and W.-Z. Chen, "A 3–10 GHz, 14 Bands CMOS Frequency Synthesizer with Spurs Reduction for MB-OFDM UWB System," *IEEE Transactions on Very Large Scale Integration (VLSI) Systems*, vol. 20, no. 5, pp. 948–958, May 2012, https://doi.org/10.1109/tvlsi.2011.2134874.

[18] Charilaos Kourogiorgas and A. D. Panagopoulos, "A Rain-Attenuation Stochastic Dynamic Model for LEO Satellite Systems Above 10 GHz," *IEEE Transactions on Vehicular Technology*, vol. 64, no. 2, pp. 829–834, Feb. 2015, https://doi.org/10.1109/tvt.2014.2322119.

[19] S. A. Kanellopoulos, C. I. Kourogiorgas, A. D. Panagopoulos, S. N. Livieratos, and G. E. Chatzarakis, "Channel Model for Satellite Communication Links Above 10GHz Based on Weibull Distribution," *IEEE Communications Letters*, vol. 18, no. 4, pp. 568–571, Apr. 2014, https://doi.org/10.1109/lcomm.2014.013114.131950.

[20] C.-H. Han, Y.-H. Yoon, S.-D. Ko, M.-H. Seo, and J.-B. Yoon, "Linear frequency tuning in an LC-resonant system using a C–V response controllable MEMS varactor," *Micro and Nano Systems Letters*, vol. 5, no. 1, Sep. 2017, https://doi.org/10.1186/s40486-017-0059-5.

[21] S. Chang and S. Sivoththaman, "A Tunable RF MEMS Inductor on Silicon Incorporating an Amorphous Silicon Bimorph in a Low-Temperature Process," *IEEE Electron Device Letters*, vol. 27, no. 11, pp. 905–907, Nov. 2006, https://doi.org/10.1109/led.2006.884712.

[22] T. B. Oogarah, M. Daneshmand, R. R. Mansour, and S. Chang, "Novel low-temperature variable inductors using porous anodic alumina," *IET Microwaves, Antennas & Propagation*, vol. 5, no. 11, p. 1274, 2011, https://doi.org/10.1049/iet-map.2010.0502.

Contribution of Individual Authors to the Creation of a Scientific Article (Ghostwriting Policy)

- Nizar HABBACHI carried out the design and the simulation.
- Kamel BESBES is the supervisor.

Sources of Funding for Research Presented in a Scientific Article or Scientific Article Itself

No funding was received for conducting this study.

Conflict of Interest

The authors have no conflicts of interest to declare.